SEMARAK ILMU PUBLISHING

Journal of Advanced Research in Applied Mechanics

Journal homepage:
https://semarakilmu.com.my/journals/index.php/appl_mech/index
ISSN: 2289-7895


# Numerical Study on the Effect of Geometrical Changes on the Deformation Behaviour of Recycled Aluminium Alloy AA6061 undergoing High Velocity Impact using Hyperworks-Radioss

Irfan Alias Farhan Latif[1], Mohamad Firdaus Supardi[1], Mohd Khir Mohd Nor[1,2,*], Mohd Syazwan Abdul Samad[3], Norzarina Ma'at[1]

[1] Crashworthiness and Collisions Research Group (COLORED), Faculty of Mechanical and Manufacturing Engineering, Universiti Tun Hussein Onn Malaysia, Parit Raja, Johor, Malaysia
[2] Advanced Materials and Manufacturing Centre (AMMC), Institute for Integrated Engineering ($I^2E$), Universiti Tun Hussein Onn Malaysia, Parit Raja, Johor, Malaysia
[3] Package Design Engineering, Package Technology Development and Integration, Western Digital Corporation, Penang, Malaysia

**ARTICLE INFO**

***Article history:***
Received 15 April 2024
Received in revised form 9 June 2024
Accepted 22 June 2024
Available online 30 July 2024

***Keywords:***
Recycling aluminium alloy; finite element analysis; high-velocity impact; Taylor Cylinder Impact Test; parametric study

**ABSTRACT**

Numerical analysis is important to predict material behaviour without require an experimental implementation. This manuscript focuses on a numerical prediction establishment of a direct recycled aluminium alloys AA6061 undergoing Taylor Cylinder Impact test using Johnson-Cook model in HyperWorks Radioss. The numerical setup was first validated against the experimental data at the velocity range of 179 to 212 m/s. Good agreement between simulation and experimental data was obtained within the range that exhibits a mushrooming shape fracture mode. A parametric study was then conducted to study the deformation behaviour of the selected recycled aluminium alloys within the validated range at various geometrical settings. The analysis was made by focusing on the post-impact configuration of the projectile at different impact velocities in terms of residual length, deformed diameter, and the final length-to-diameter ratio. It was found that a broader projectile experienced a less significant reduction in its final length ($L_f/L_o$ goes from 0.87 to 0.9 for projectile diameter 9mm to 34mm) and a smaller increase in the deformed diameter compared to a thinner projectile ($D_f/D_o$ goes from 1.18 to 1.12 for projectile diameter 9mm to 34mm). It was found that a thinner projectile experienced more diameter expansion than length reduction post impact. In addition, a longer projectile experienced more residual length reduction ($L_f/L_o$ goes from 0.92 to 0.87 for projectile length 2mm to 14mm) and more radial deformation compared to the one with a smaller initial length ($D_f/D_o$ goes from 1.06 to 1.18 for projectile length 2mm to 14mm). All projectiles showed more significant changes on the deformed diameter compared to the changes in residual length post-impact. The results helped the understanding of a critical aspect of the deformation behaviour of recycled aluminium alloy AA6061 more effectively compared to experimental work implementation.

* *Corresponding author.*
*E-mail address: khir@uthm.edu.my*

https://doi.org/10.37934/aram.121.1.91106

## 1. Introduction

Aluminium alloys offer several advantages, including lightweight, high strength-to-weight ratio, corrosion resistance, high thermal and electrical conductivity, and ease of fabrication. These properties make aluminium alloys ideal for various applications in the aerospace, automotive, construction, packaging, and electronics industries. The alloys can be easily formed into different shapes and are resistant to environmental degradation, making them suitable for use in harsh environments. Therefore, various efforts have been made to characterize aluminium alloys to accommodate various industrial applications [1-5].

However, the manufacturing processes of the primary aluminium alloys have negative impacts on the environment. One such impact is the energy consumption associated with the production of aluminium alloys, which contributes to greenhouse gas emissions and climate change. Another disadvantage is the release of toxic pollutants and waste products during the refining and smelting of aluminium alloys, which can harm local water and air quality. Additionally, the production of aluminium alloys often involves the use of hazardous chemicals, which can be harmful to both workers and the environment if not handled and disposed of properly. The bauxite mining process, used to obtain the raw material for aluminium production, can also have negative impacts on the environment, such as deforestation, soil degradation, and the displacement of local communities.

Luckily aluminium alloys show recyclability potential which offers a significant positive impact on the environment by reducing the amount of industrial waste produced, conserving energy and natural resources, and reducing greenhouse gas emissions. By recycling aluminium alloys, the amount of waste that is generated and sent to landfills is reduced. This helps to conserve space in landfills and minimize environmental damage from waste disposal. Recycling aluminium requires only a fraction of the energy needed to produce primary aluminium from raw materials. This can result in a significant reduction in energy consumption, which in turn reduces greenhouse gas emissions from energy production. By recycling aluminium, the need for new aluminium production is also reduced to solve a supply chain issue of primary aluminium alloys by reducing the demand for newly mined aluminium and conserving natural resources, leading to a reduction in greenhouse gas emissions.

In recent years, there have been a lot of efforts conducted focusing on various recycling processes aluminium alloys such as dry ball milling, powder metallurgy, cold compression, compressive torsion processing, hot extrusion, and hot press forging to recycle aluminium scrap or chips [6-14]. There is still room to further optimize the recycling parameters for the various techniques to achieve better microstructure, wear resistance, and mechanical properties in the recycled aluminium alloys. Another potential area is the development of new techniques for removing impurities and contaminants from recycled aluminium chips, which could potentially improve the quality of the final product. Following this, numerical simulations can be used to model and predict the behaviour of aluminium alloys during different stages of the recycling process, such as milling and extrusion. This can help researchers to optimize the process parameters to identify the optimal conditions for producing high-quality recycled aluminium.

It can be observed that the finite element method is widely used for predicting stress-strain behaviour when structures or components are subjected to mechanical or thermal loading [15-22]. There have been many published studies on the effects of strain rates and temperatures on material behaviour, including the Johnson-Cook model, Mechanical Threshold Stress (MTS), and Zerilli-Armstrong (Z-A) models. Researchers have used numerical analysis to investigate the flow stress behaviour and evaluate the impact of strain rates and temperatures [23-25]. In industrial applications, the Johnson-Cook model is widely incorporated into numerical simulation tools because

the model constants can be characterized more easily [26]. Murugesan and Jung [26] used the Johnson-Cook model, including a damage model, to characterize the flow stress behaviour of AISI-1045 medium carbon steel at elevated temperatures and a range of strain rates. The model constants were determined using tensile test data, and a good agreement was obtained between experimental and simulation results. Grazka and Janiszewski [27] used the Johnson-Cook model to predict the deformation behaviour of copper Cu-ETP under the Taylor Cylinder Impact test and determined the model constants with the help of ANSYS Autodyn software. The results showed that the modified Johnson-Cook model provides a more accurate description of the flow stress behaviour of the material under different temperature and strain rate conditions. Many other studies have used the Johnson-Cook model, including Vedantam *et al.,* [28] for mild and DP steels, Banerjee *et al.,* [29] for armour steel, Majzoobi and Dehgolan [30], and so on. In most of these studies, the simulation results showed a good agreement with the experimental results, confirming the ability of the Johnson-Cook model to predict material deformation behaviour.

Modifications have also been made to the Johnson-Cook model to improve its ability to predict material deformation behaviour. For example, Gambirasio and Rizzi [31] implemented the Split Johnson-Cook strength model for structural steel, pure metal, and stainless steel and found that this new model provided better results than the original Johnson-Cook model. Zhao *et al.,* [32] compared the performance of the original and modified Johnson-Cook models for a laser additive manufacturing FeCr alloy and found that the modified model, which considered thermal softening and strain rate hardening, improved the accuracy of the original model. Stopel and Skibicki [24] used a simplified Johnson-Cook model to characterize material deformation behaviour under the Charpy test using LS-DYNA and obtained satisfactory results.

As discussed above, various efforts can be seen in numerical simulations aimed at predicting the deformation of primary aluminium alloys undergoing finite strain deformation including modelling at high-velocity impact [33,34]. Despite various attempts, predicting the deformation behaviour of recycled aluminium alloys remains a challenge. This is due to the need for a significant amount of experimental data, despite the significant characterization work that has already been performed [35,36]. To date, the only effort that can be found was made by Ho *et al.,* [37] where the authors aimed to model the temperature and strain-rate dependence of recycled aluminium alloy AA6061 under different quasi-static strain rates ranging from $1\times10^{-4}$ $s^{-1}$ to $1\times10^{-3}$ $s^{-1}$, at elevated temperatures of 100 °C, 200 °C, and 300 °C. The study provides valuable information for researchers in the field of materials science and engineering, as it helps to improve the understanding to model the behaviour of recycled aluminium alloys under various conditions. Conversely, pertaining to the primary aluminium alloy, efforts can be found in literature such as Nor [38], where a constitutive model is prepared to predict the deformation behaviour of commercial aluminium alloy AA 7010 subjected to high-velocity impact.

At higher strain rate levels, the Taylor Cylinder Impact test has long been used as a standard method to assess the constitutive behaviour of materials [39]. This test has been refined in several research studies [40,41]. This test involves striking a short, right-circular cylinder with a length-to-diameter (L/D) ratio against a rigid, massive wall [42]. One of the researchers used this test to analyse the deformation and fracture modes of steel projectiles during impact [43]. The results showed several fracture modes, including mushrooming, void nucleation, tensile splitting, principal shear crack, spiral shear, tensile splitting, and fragmentation. These various deformations and fracture modes were attributed to the impact velocity and hardness of the projectiles [44,53]. All projectiles that had an impact velocity lower than the critical velocity experienced mushrooming, while projectiles with higher impact velocities experienced deformation related to damage fracture [43]. In [45], the damage behaviour of recycled aluminium alloys AA 6061 undergoing high-velocity impact

was characterized using the Taylor cylinder impact test. The deformation was found to be anisotropic in nature. However, there is no effort has been made to investigate the geometrical effects on the deformation behaviour of recycled aluminium alloys, mainly due to costly experimental works. The advancement of numerical modelling can help to improve the understanding more efficiently.

Previous researchers have utilized various plastic deformation and plasticity models, including the classic Von Mises criterion, Johnson-Cook model, Steinburg-Guinan, and Zerilli-Armstrong model, to simulate the Taylor Cylinder Impact test [46]. The Johnson-Cook model is commonly used in analyzing high-velocity impact, fracture, and deformation in materials [47-51]. One advantage of using the Johnson-Cook model in finite element analysis is that it considers strain, strain rate, and temperature simultaneously and proportionally to the predicted flow stress [52].

In this study, numerical simulation was conducted to predict the deformation behaviour of recycled aluminium alloys at the high-velocity impact of the Taylor Cylinder Impact test using the Johnson-Cook model using HyperWorks Radioss. The numerical model was validated against experimental data presented in [35] to demonstrate the predictive capability of the developed finite element method. Based on the agreement observed in validation, a parametric study was then conducted to analyze the effects of the length-to-diameter (L/D) ratio on the deformation behaviour of this sustainable material subjected to high-velocity impact. This study is crucial for establishing the deformation behaviour of recycled aluminium alloys under various geometrical settings within the validated range.

## 2. Methodology

Figure 1 shows the FE model developed using HyperWorks. A full cylindrical shape of the projectile is developed. A flat-faced cylinder with a 15 mm length x 8.45 mm diameter is developed identically to the geometry adopted in the experimental test. Automesh was used to generate an appropriate mesh for the created geometry. The final mesh consists of 19833 nodes and 19200 solid elements. Table 1 shows the material properties of recycled AA6061 used in this study.

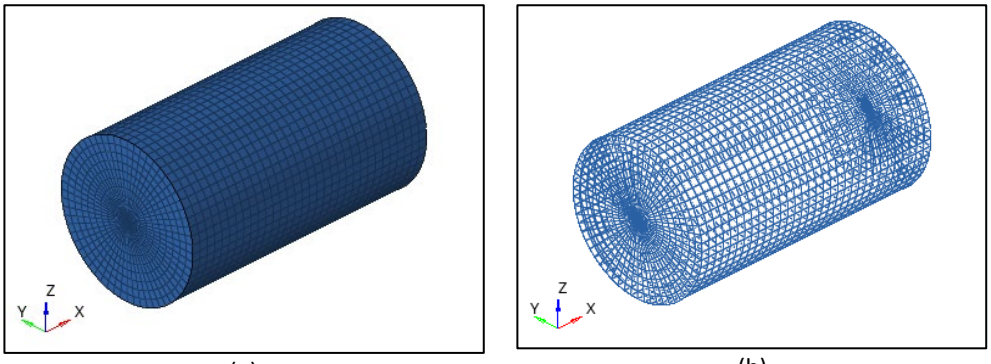


(a) (b)

**Fig. 1.** Geometry development of the projectile. (a) model (b) meshing

**Table 1**
Properties of Recycled Aluminium Alloys AA6061 [35]

| Temperature (˚C) | Density (tonne/mm$^3$) | Poisson Ratio | Strain rate (s$^{-1}$) | Elastic modulus (GPa) |
|---|---|---|---|---|
| 200 | $2.69\times 10^{-9}$ | 0.33 | 0.0005 | 62.61 |

In this study, the material model M2_PLAS_JOHNS_ZERIL of a Simplified Johnson-Cook model is adopted with the inclusion of the damage parameter. Table 2 shows the parameters of the simplified Johnson-Cook model of the recycled AA6061. For property assignment, P14_SOLID is used.

**Table 2**
Simplified Johnson-Cook parameters of recycled AA6061 [37]

| Parameters | Value |
|---|---|
| Yield stress constant, A | 143.28 MPa |
| Strain rate hardening constant, B | 1046.81 MPa |
| Strain hardening coefficient, n | 0.7641 |
| Strain rate coefficient, C | -0.0129 |

The finite modelling of the Taylor impact test involves impacting the projectile towards the rigid wall. Thus, a point velocity needs to be assigned to the projectile to represent the impact velocity. Figure 2 shows the assignment of impact velocity on the projectile. The wall as mentioned above is made rigid, while the bullet is a deformable solid body. The last step in modelling the Taylor cylinder impact test was the creation of a rigid wall. In this study, the rigid wall is created by using an infinite plane centered at the origin (0,0,0), thus, the assignment of a rigid boundary is unnecessary. The linear axis of motion for the projectile is set in the x-direction. The digitized data of the deformed footprint, major profile, and side profile will be taken at the y-z, x-y, and x-z planes, respectively. Figure 3 illustrates the finite element model of the Taylor cylinder impact test. Contact Type 7 was used as it is generally utilized for two bodies in contact.

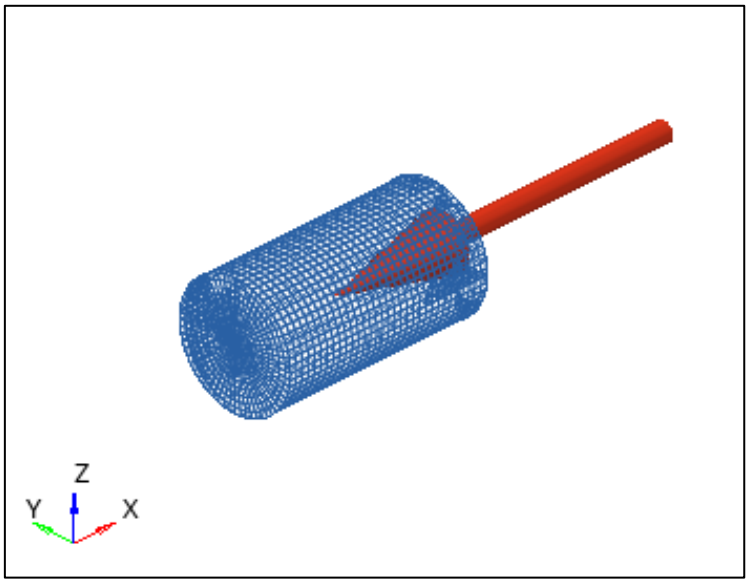


**Fig. 2.** Assignment of impact velocity on the projectile

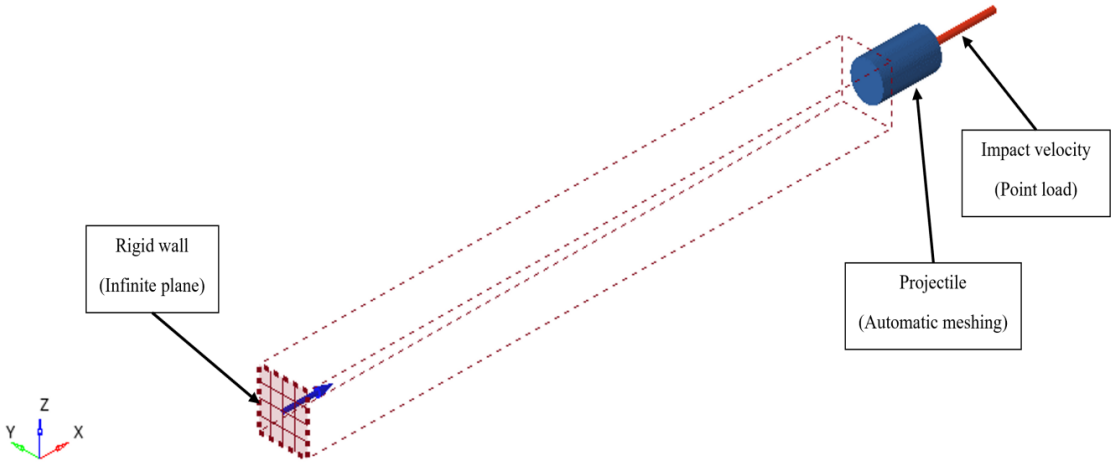


**Fig. 3.** Finite element model

## 3. Validation of the Numerical Model

Table 3 presents the published data used to validate the numerical model. The impact data adopted in this analysis was limited to a fracture mode governed only by plastic strain deformation of a mushrooming shape. This is due to the absence of damage and equation of state (EOS) that limits the capability of the numerical analysis to accurately predict the fracture mode beyond mushrooming shape.

**Table 3**
Impact behaviour of recycled AA6061 [35]

| Initial velocity, V (m/s) | Final length, $L_f$ (mm) | Distance of major profile, $D_d$ (mm) | Fracture mode |
|---|---|---|---|
| 179.01 | 13.84 | 10.09 | Mushrooming |
| 195.28 | 13.58 | 10.65 | Mushrooming |
| 212.35 | 13.48 | 10.24 | Mushrooming |

Figure 4 shows the comparison between the experiment and simulation in terms of the deformed footprint around the impact area. As can be seen, the data referring to length reduction also provides the configuration of side profile deformation of the deformed cylinder. For the digitized data, the red line represents the impacted surface obtained from the simulation, while the blue line denotes the impacted surface obtained from the experiment. By direct observations, both deformed footprints are nearly identical, while the major profile shows slight differences.

Table 4 and Table 5 summarize the analysis results of the validation stage. In Table 4, the simulation results showed slight differences from the experimental results, which are 0.59%, 1.78%, and 3.91% for each impact velocity in terms of the diameter of the major profile. In terms of length reduction, the difference between the experiment and simulation results are only 0.49 mm., 0.47 mm, and 0.56 mm for each impact velocity, as taken in Table 5 accordingly.

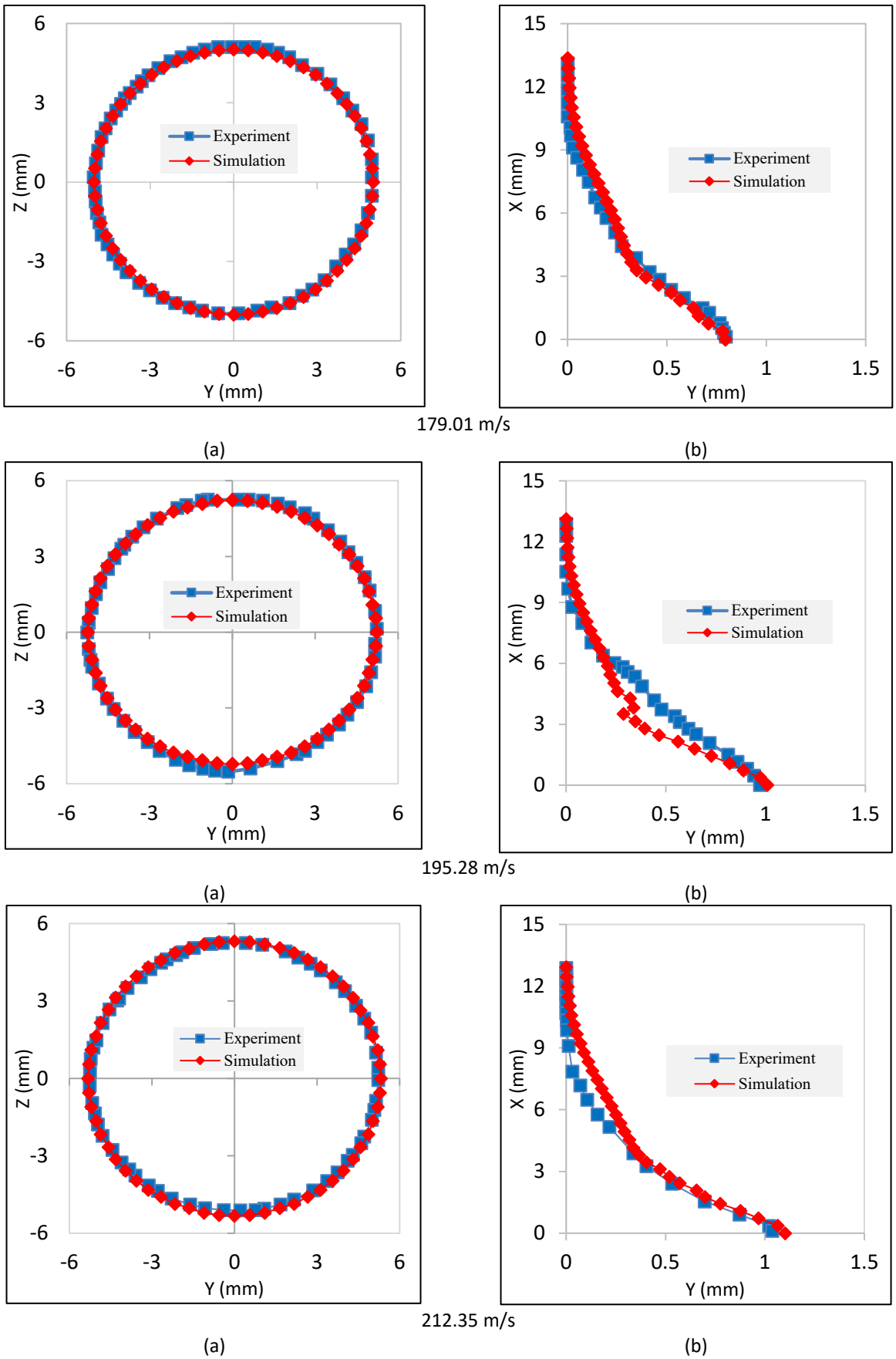


**Fig. 4.** Comparison between experiment and simulation at various impact velocities (a) deformed footprint (b) side profile

**Table 4**
Comparison of the diameter of major profile between experiment and simulation

| Impact velocity, V (m/s) | Diameter of the major profile, $D_d$ (mm) | |
|---|---|---|
| | Experiment | Simulation |
| 179.01 | 10.09 | 10.03 |
| 195.28 | 10.65 | 10.46 |
| 212.35 | 10.24 | 10.24 |

**Table 5**
Comparison of final length and length reduction between experiment and simulation

| Impact velocity, V (m/s) | Final length, $L_f$ (mm) | | Length reduction, $\Delta L$ (mm) | |
|---|---|---|---|---|
| | Experiment | Simulation | Experiment | Simulation |
| 179.01 | 13.84 | 13.35 | 1.16 | 1.65 |
| 195.28 | 13.58 | 13.11 | 1.42 | 1.89 |
| 212.35 | 13.48 | 12.92 | 1.52 | 2.08 |

The results were good enough to conclude that there is a good agreement between the simulation results and experimental data within the tested range. Thus, this model is used to predict the behaviour of varying geometric configurations of the recycled AA 6061 undergoing Taylor cylinder impact test within this range of velocities.

## 4. Parametric Study

The parametric studies consist of an alteration of initial diameter and initial length to analyze their effects on the final configuration of the projectile. Both studies adopted the same length-to-diameter ratio, L/D ranging from 0.25 to 1.75 with an increment of 0.10. For the alteration of initial length, the L/D ratio was varied by increasing the initial diameter from 9.09 mm to 33.33 mm while keeping the initial length constant at 15.00 mm. On the contrary, the L/D ratio for alteration of initial length was varied by decreasing the initial length from 14.80 mm to 2.11 mm while keeping the initial diameter constant at 8.45 mm. The test matrix for parametric studies involving changes to the initial diameter and initial length of the specimen is shown in Tables 6 and 7, respectively.

**Table 6**
Test matrix for parametric studies involving changes to the initial diameter

| Test No. | Length to diameter ratio, L/D | Alteration of initial diameter, $D_o$ (mm) with fixed initial length $L_o$ = 15 (mm) |
|---|---|---|
| 1 | 1.65 | 9.09 |
| 2 | 1.55 | 9.68 |
| 3 | 1.45 | 10.34 |
| 4 | 1.35 | 11.11 |
| 5 | 1.25 | 12.00 |
| 6 | 1.15 | 13.04 |
| 7 | 1.05 | 14.29 |
| 8 | 0.95 | 15.79 |
| 9 | 0.85 | 17.65 |
| 10 | 0.75 | 20.00 |
| 11 | 0.65 | 23.08 |
| 12 | 0.55 | 27.27 |
| 13 | 0.45 | 33.33 |

**Table 7**
Test matrix for parametric studies involving changes to the initial length

| Test No. | Length to diameter ratio, L/D | Alteration of initial length, $L_o$ (mm) with fixed Initial diameter, $D_o$ = 8.45 (mm) |
|---|---|---|
| 1 | 1.75 | 14.80 |
| 2 | 1.65 | 13.95 |
| 3 | 1.55 | 13.10 |
| 4 | 1.45 | 12.25 |
| 5 | 1.35 | 11.40 |
| 6 | 1.25 | 10.55 |
| 7 | 1.05 | 8.87 |
| 8 | 0.95 | 8.03 |
| 9 | 0.85 | 7.18 |
| 10 | 0.75 | 6.34 |
| 11 | 0.65 | 5.49 |
| 12 | 0.55 | 4.65 |
| 13 | 0.45 | 3.80 |
| 14 | 0.35 | 2.96 |
| 15 | 0.25 | 2.11 |

The result of the numerical analysis, including the validation of the preliminary data and the parametric studies, was summarized in the following section.

### *4.1 Results and Discussion*

In the parametric studies, the post-impact configuration of the projectile is defined in terms of residual length ($L_f/L_o$), and deformed diameter ($D_f/D_o$). Figure 5, Figure 6, and Figure 7 present the final configuration of the deformed projectile using a variation of the initial diameter. In contrast, Figure 8, Figure 9, and Figure 10 illustrate the final configuration using a variation of initial length. Both settings were tested at different impact velocities; 179.01, 195.28 and 212.35 m/s.

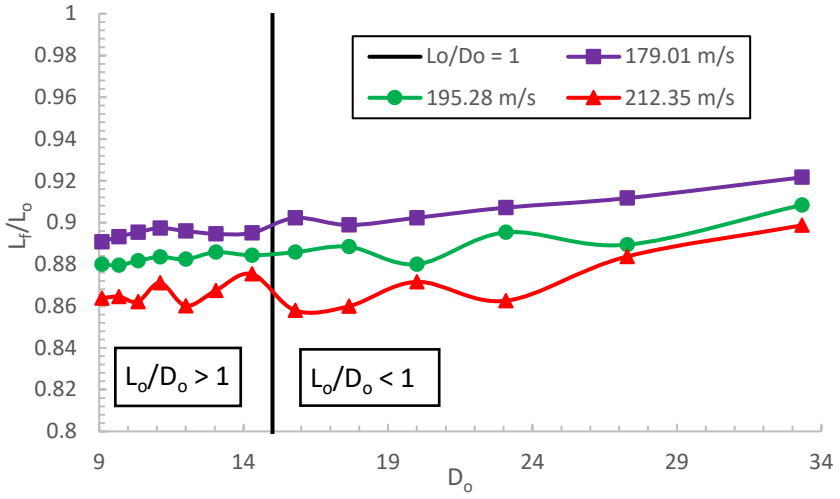


**Fig. 5.** Comparison of the residual length vs initial diameter

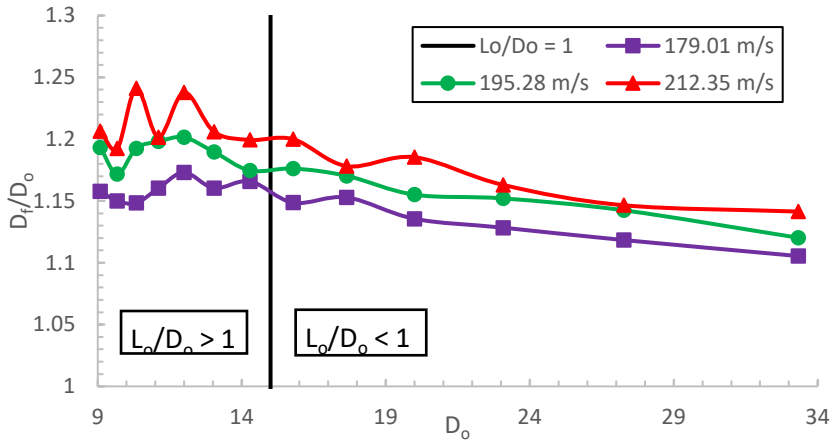


**Fig. 6.** Comparison of the deformed diameter vs initial diameter

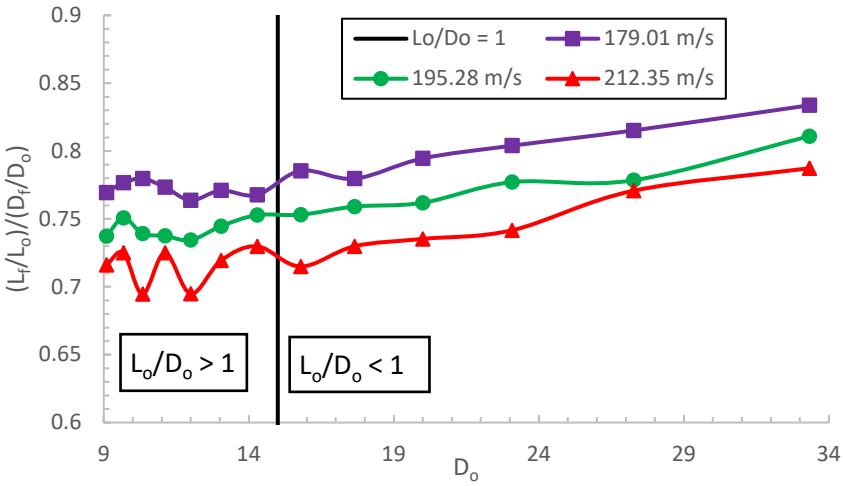


**Fig. 7.** Comparison of the residual length over the deformed diameter vs initial length

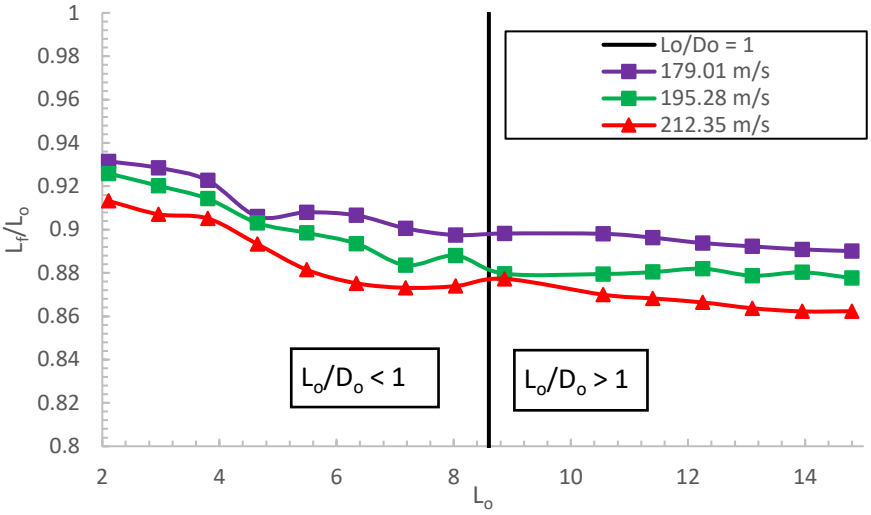


**Fig. 8.** Comparison of the residual length vs initial length

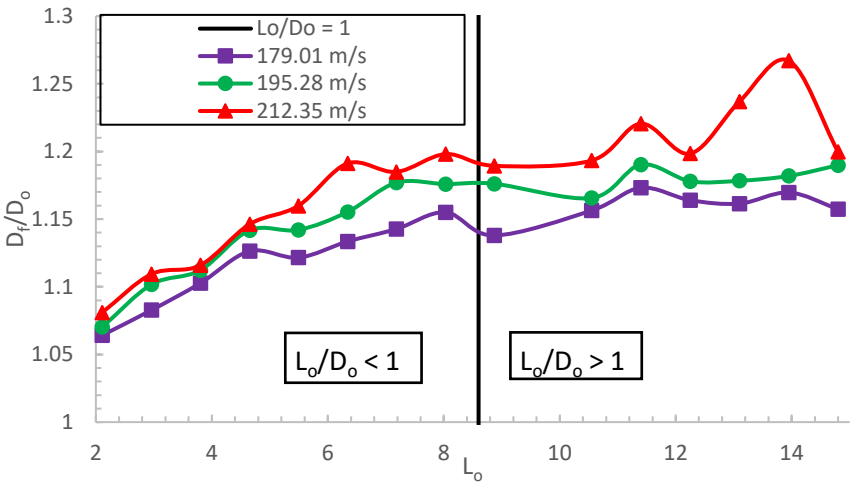


**Fig. 9.** Comparison of the deformed diameter vs initial length

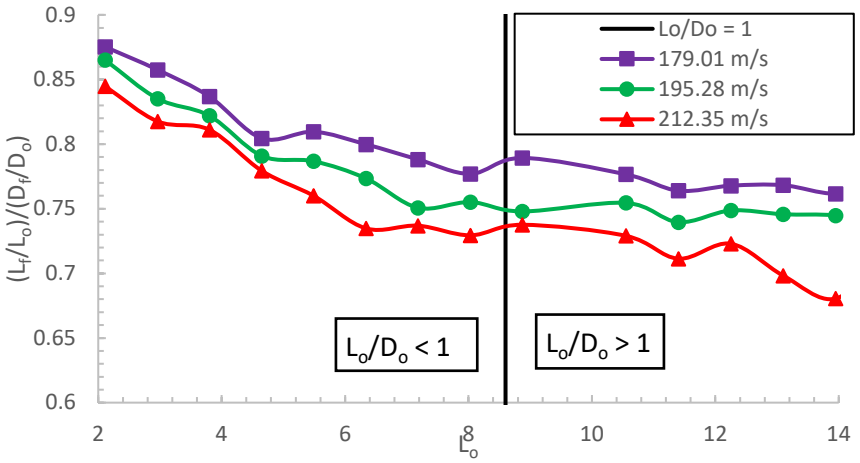


**Fig. 10.** Comparison of the residual length over the deformed diameter vs initial length

### *4.1.1 Effect of the initial diameter changes on the final configuration*

In this section, the change in residual length ($L_f$) and deformed diameter ($D_f$) with respect to the change in initial diameter ($D_o$) post-impact are presented. Figure 5 exhibits that, increasing the initial diameter value may cause the residual length to initial length ratio ($L_f/L_o$) to approach 1 from values lower than 1. This shows that a broader projectile experienced a less significant reduction in final length compared to a thinner projectile. This effect is prominently observed in specimens having a $L_o/D_o$ ratio below 1.0 (where the diameter of the projectile is greater than its length). While for the specimen having a $L_o/D_o$ ratio above 1 (where the length of the projectile is greater than its diameter), the change in final length with respect to diameter is observed at a smaller degree. This trend holds at all tested velocities. Additionally, with an increase in velocity, a more significant reduction in residual length is observed.

In radial deformation, as depicted in Figure 6, it can be observed that increasing the initial diameter causes the deformed diameter to initial diameter ratio ($D_f/D_o$) to decrease for specimens with $L_o/D_o$ ratio below 1. The ratio tends to approach 1 from values above 1. This concludes that a broader projectile will undergo a smaller increase in the deformed diameter after impact. For specimens with $L_o/D_o$ ratio above 1, no clear trend is observed. In some instances, such as going from

a $D_o$ of 9.09mm to 10.34mm at 212 m/s, the ratio $D_f/D_o$ increases, while with a subsequent increase of $D_o$ to 11.11mm, it reduces. In general, the ratio $D_f/D_o$ seem to hover around the same region for a specimen having a $L_o/D_o$ ratio above 1 with minimal changes limited to a factor of about 0.05, suggesting a minimal change in deformed diameter post-impact with respect to change in initial diameter with no clear trend. Additionally, $D_f/D_o$ ratio is observed to be increasing with an increase in impact velocity.

Finally, figure 7 compares the residual length change ($L_f/L_o$) to the deformed diameter change ($D_f/D_o$). All of the specimens result in values lower than 1. This means that all projectiles undergo more significant changes in deformed diameter compared to changes in residual length post-impact. From the specimen having a $L_o/D_o$ ratio below 1, a clear trend is observed at all velocities as the ratio $\{(L_f/L_o)/ (D_f/D_o)\}$ is observed to be approaching 1 from values lower than 1 with an increase in initial diameter. This suggests that a broader projectile will observe length reduction to a more similar degree/extent as the final diameter increase. However, in all cases, the changes in deformed diameter outweigh the changes to the residual length. Similar to previous observations, no clear trend is observed in specimens with $L_o/D_o$ ratio above 1. The changes in value occur at a maximum scale of 0.03 while most of the speciments hover around 0.75.

### *4.1.2 Effect of the initial length changes on the final configuration*

In this section, the effect on residual length ($L_f$) and deformed diameter ($D_o$) with respect to changes in initial length ($L_o$) are shown. First, as shown in Figure 8, increasing the initial length value will cause the residual length to initial length ratio ($L_f/L_o$) to decrease to values below 1. This shows that a projectile having a shorter length experienced a lower reduction in the final length. Conversely, a projectile with a larger initial length experienced more residual length reduction. This trend is observed in both types of specimens (ones having a $L_o/D_o$ above 1 and the ones having a $L_o/D_o$ below 1). However, it is more prominently observed in specimens with a $L_o/D_o$ below 1. Additionally, increasing the velocity will result in a more significant final length reduction.

According to Figure 9, increasing the initial length caused the deformed diameter to initial diameter ratio ($D_f/D_0$) to increase from values above 1. This result indicates that larger projectile experiences more radial deformation compared to a smaller one. Increasing the velocity results in more radial deformation.

Figure 10 compares the residual length change ($L_f/L_o$) to the deformed diameter change ($D_f/D_o$). As observed in Figure 7, all of the specimens result in values lower than 1. This means that all projectiles undergo more significant changes in deformed diameter compared to changes in residual length post-impact. In Figure 7, an increase in the ratio of residual length to deformed diameter was observed with increasing initial diameter. However, when increasing the initial length, the ratio decreases to values lower than 1. Suggesting a longer projectile undergoes much more radial deformation compared to smaller ones.

## 5. Conclusion

This research investigates and models the deformation behavior of recycled aluminium alloys undergoing finite strain deformation and analyzes the effects of parametric studies on recycled aluminium alloys at high-velocity impact. During the validation stage, the numerical analysis could predict three modes of fracture, including mushrooming, tensile splitting with cracks, and petalling at various impact velocities. The digitized data of the deformed footprint, major profile, and side profile of the simulation possess remarkable similarities with the experimental results, which proves

that the selected Johnson-Cook model and the inclusion of damage parameters are capable of validating the preliminary data. However, it is limited to the mushrooming mode only due to the absence of equation of state (EOS) activation. The validated numerical settings are then used to conduct the parametric studies to analyze the effect of geometrical alteration on the final configuration of the projectile made of recycled aluminium alloys. These types of parametric studies are crucial in establishing the behaviour/properties of a relatively new material such as the recycled AA 6061 obtained through hot press forging. Generally, these studies would require extensive experimentation to investigate the desired relationship between the behaviour of the material and the geometrical alterations. But, through FEA, we can reasonably predict the behaviour up to a verified range.

The following trends are observed from the parametric studies carried out in this work:

i. A Broader projectile experienced a less significant reduction in final length and a smaller increase in the deformed diameter compared to a thinner one.
ii. A broader projectile will observe length reduction to a more similar degree/extent as the final diameter increase compared to a thinner one.
iii. A projectile with a larger initial length experienced more residual length reduction and more radial deformation.
iv. A longer projectile undergoes much more radial deformation compared to smaller ones.
v. All projectiles undergo more significant changes in deformed diameter compared to changes in residual length post-impact.

The results of this FEA can be used as the baseline for further enquiry into the behaviour of the material undergoing Taylor cylinder impact tests. With a better numerical model, a wider range of velocities can be tested in the future. The results for recycled AA 6061 can be compared with the primary AA 6061 undergoing the same tests to help establish where the recycled counterpart of the AA 6061 alloy stacks up compared to the primary form. This intern will help identify some practical uses for the material. Additionally, the impact perforation behaviour or resistance can be investigated for this material with slight changes to the model as the dynamics for perforation tests and Taylor cylinder impact tests are similar.

**Acknowledgement**
The authors wish to convey sincere gratitude to the Ministry of Higher Education Malaysia (MOHE) for providing the financial means during the preparation to complete this work under Fundamental Research Grant Scheme (FRGS/1/2020/TK02/UTHM/02/5), FRGS Vot K331.

**References**

[1] Ismail, A. E., S. H. Masran, S. Jamian, K. A. Kamarudin, MK Mohd Nor, NH Muhd Nor, AL Mohd Tobi, and M. K. Awang. "Fracture toughness of woven kenaf fibre reinforced composites." In *IOP Conference Series: Materials Science and Engineering*, vol. 160, no. 1, p. 012020. IOP Publishing, 2016. https://doi.org/10.1088/1757-899X/160/1/012020

[2] Ma'at, Norzarina, MK Mohd Nor, Choon Sin Ho, N. Abdul Latif, Al Emran Ismail, K. A. Kamarudin, S. Jamian, M. Norihan Ibrahim, and M. Khairudin Awang. "Effects of temperatures and strain rate on the mechanical behaviour of commercial aluminium alloy AA6061." *Journal of Advanced Research in Fluid Mechanics and Thermal Sciences* 54, no. 2 (2019): 185-190.

[3] Mohd Nor, Mohd Khir, and Ibrahim Mohamad Suhaimi. "Effects of temperature and strain rate on commercial aluminum alloy AA5083." *Applied Mechanics and Materials* 660 (2014): 332-336. https://doi.org/10.4028/www.scientific.net/AMM.660.332

[4] Mahli, Maximus Kohnizio, Saifulnizan Jamian, Nik Hisyamudin Muhd Nor, Mohd Khir Mohd Nor, and Kamarul Azhar Kamarudin. "Effect of Rotating Mold Speed on Microstructure of Al LM6 Hollow Cylinder Fabricated Using Centrifugal Method." In *Journal of Physics: Conference Series*, vol. 914, no. 1, p. 012039. IOP Publishing, 2017. https://doi.org/10.1088/1742-6596/914/1/012039

[5] Hong, Seong-Hyeon, Dong-Won Lee, and Byoung-Kee Kim. "Manufacturing of aluminum flake powder from foil scrap by dry ball milling process." *Journal of Materials Processing Technology* 100, no. 1-3 (2000): 105-109. https://doi.org/10.1016/S0924-0136(99)00469-0

[6] Kumar, Shivendra, Fabrice Mathieux, Godfrey Onwubolu, and Vineet Chandra. "A novel powder metallurgy-based method for the recycling of aluminum adapted to a small island developing state in the Pacific." *International Journal of Environmentally Conscious Design & Manufacturing* 13, no. 3, 4 (2007): 1-22.

[7] Rahimian, Mehdi, Nader Parvin, and Naser Ehsani. "The effect of production parameters on microstructure and wear resistance of powder metallurgy Al–Al2O3 composite." *Materials & Design* 32, no. 2 (2011): 1031-1038. https://doi.org/10.1016/j.matdes.2010.07.016

[8] Rahimian, Mehdi, Naser Ehsani, Nader Parvin, and Hamid reza Baharvandi. "The effect of particle size, sintering temperature and sintering time on the properties of Al–Al2O3 composites, made by powder metallurgy." *Journal of Materials Processing Technology* 209, no. 14 (2009): 5387-5393. https://doi.org/10.1016/j.jmatprotec.2009.04.007

[9] Chan, B. L., and M. A. Lajis. "Direct recycling of aluminium 6061 chipThrough cold compression." *Int. J. Eng. Technol* 15, no. 04 (2015): 4-8.

[10] Kume, Yuji, Takashi Takahashi, Makoto Kobashi, and Naoyuki Kanetake. "Solid state recycling of die-cast aluminum alloy chip wastes by compressive torsion processing." *Keikinzoku/Journal Japan Inst. Light Met* 59, no. 7 (2009): 354-358. https://doi.org/10.2464/jilm.59.354

[11] Ab Rahim, Syaiful Nizam, Mohd Zaniel Mahadzir, Nik Ahmad Faris Nik Abdullah, and Mohd Amri Lajis. "Effect of Extrusion Ratio of Recycling Aluminium AA6061 Chips by the Hot Extrusion Process." *International Journal of Advanced Research in Engineering Innovation* 1, no. 2 (2019): 15-20.

[12] Haase, Matthias, and A. Erman Tekkaya. "Recycling of aluminum chips by hot extrusion with subsequent cold extrusion." *Procedia Engineering* 81 (2014): 652-657. https://doi.org/10.1016/j.proeng.2014.10.055

[13] Rahim, S. N. A., M. A. Lajis, and S. Ariffin. "Effect of extrusion speed and temperature on hot extrusion process of 6061 aluminum alloy chip." *ARPN J. Eng. Appl. Sci* 11, no. 4 (2016): 2272-2277.

[14] Tekkaya, A. E., M. Schikorra, D. Becker, D. Biermann, N. Hammer, and K. Pantke. "Hot profile extrusion of AA-6060 aluminum chips." *Journal of materials processing technology* 209, no. 7 (2009): 3343-3350. https://doi.org/10.1016/j.jmatprotec.2008.07.047

[15] Jamian, Saifulnizan, Kamarul Azhar Kamarudin, Mohd Khir Mohd Nor, Mohd Norihan Ibrahim, and Moch Agus Choiron. "An overview of fracture mechanics with ANSYS." *International Journal of Integrated Engineering* 10, no. 5 (2018).

[16] Mohd Nor, Mohd Khir, Rade Vignjevic, and James Campbell. "Plane-stress analysis of the new stress tensor decomposition." *Applied Mechanics and Materials* 315 (2013): 635-639. https://doi.org/10.4028/www.scientific.net/AMM.315.635

[17] Nor, MK Mohd. "Modelling inelastic behaviour of orthotropic metals in a unique alignment of deviatoric plane within the stress space." *International Journal of Non-Linear Mechanics* 87 (2016): 43-57. https://doi.org/10.1016/j.ijnonlinmec.2016.09.011

[18] Mohd Nor, M. K., N. Ma'at, and C. S. Ho. "An anisotropic elastoplastic constitutive formulation generalised for orthotropic materials." *Continuum Mechanics and Thermodynamics* 30 (2018): 825-860. https://doi.org/10.1007/s00161-018-0645-7

[19] Rahman, Muhammad Faisal Abdul, Kamarul Azhar Kamarudin, Hendery Dahlan, and Mohamed Nasrul Mohamed Hatta. "Ballistic Limit Prediction On Nacre Shell Using Numerical Simulation Approach." *Advanced Research in Natural Fibers* 2, no. 1 (2020): 25-29.

[20] Zahrin, Muhammad Fadhli, Kamarul-Azhar Kamarudin, and Ahmad Sufian Abdullah. "Numerical simulation of oblique impact on structure using finite element method." In *AIP Conference Proceedings*, vol. 2644, no. 1. AIP Publishing, 2022. https://doi.org/10.1063/5.0106753

[21] Kamarudin, Kamarul Azhar, and Iskandar Abdul Hamid. "Effect of high velocity ballistic impact on pretensioned carbon fibre reinforced plastic (CFRP) plates." In *IOP conference series: materials science and engineering*, vol. 165, no. 1, p. 012005. Iop Publishing, 2017. https://doi.org/10.1088/1757-899X/165/1/012005

[22] Ariffin, Nuruddin, Kamarul-Azhar Kamarudin, Ahmad Sufian Abdullah, and Mohd Idrus Abd Samad. "Crash Investigation on Frontal Vehicle Chassis Frame using Finite Element Simulation." *Journal of Advanced Research in Applied Sciences and Engineering Technology* 28, no. 2 (2022): 124-134. https://doi.org/10.37934/araset.28.2.124134

[23] Panov, Vili. "Modelling of behaviour of metals at high strain rates." (2006). https://doi.org/10.1063/1.2263405
[24] Stopel, Michał, and Dariusz Skibicki. "Determination of Johnson-Cook model constants by measurement of strain rate by optical method." In *AIP conference proceedings*, vol. 1780, no. 1. AIP Publishing, 2016. https://doi.org/10.1063/1.4965956
[25] Banerjee, Biswajit. "The mechanical threshold stress model for various tempers of AISI 4340 steel." *International journal of solids and structures* 44, no. 3-4 (2007): 834-859. https://doi.org/10.1016/j.ijsolstr.2006.05.022
[26] Murugesan, Mohanraj, and Dong Won Jung. "Johnson Cook material and failure model parameters estimation of AISI-1045 medium carbon steel for metal forming applications." *Materials* 12, no. 4 (2019): 609. https://doi.org/10.3390/ma12040609
[27] Grązka, Michał, and Jacek Janiszewski. "Identification of Johnson-Cook equation constants using finite element method." *Engineering Transactions* 60, no. 3 (2012): 215-223.
[28] Vedantam, K., D. Bajaj, N. S. Brar, and S. Hill. "Johnson-Cook strength models for mild and DP 590 Steels." In *AIP conference proceedings*, vol. 845, no. 1, pp. 775-778. American Institute of Physics, 2006. https://doi.org/10.1063/1.2263437
[29] Banerjee, A., S. Dhar, S. Acharyya, D. Datta, and N. Nayak. "Determination of Johnson cook material and failure model constants and numerical modelling of Charpy impact test of armour steel." *Materials Science and Engineering: A* 640 (2015): 200-209. https://doi.org/10.1016/j.msea.2015.05.073
[30] Majzoobi, G. H., and F. Rahimi Dehgolan. "Determination of the constants of damage models." *Procedia Engineering* 10 (2011): 764-773. ttps://doi.org/10.1016/j.proeng.2011.04.127
[31] Gambirasio, Luca, and Egidio Rizzi. "An enhanced Johnson–Cook strength model for splitting strain rate and temperature effects on lower yield stress and plastic flow." *Computational Materials Science* 113 (2016): 231-265. https://doi.org/10.1016/j.commatsci.2015.11.034
[32] Zhao, Yanhua, Jie Sun, Jianfeng Li, Yuqin Yan, and Ping Wang. "A comparative study on Johnson-Cook and modified Johnson-Cook constitutive material model to predict the dynamic behavior laser additive manufacturing FeCr alloy." *Journal of Alloys and Compounds* 723 (2017): 179-187. https://doi.org/10.1016/j.jallcom.2017.06.251
[33] Mohd Nor, M. K., C. S. Ho, N. Ma'at, and M. F. Kamarulzaman. "Modelling shock waves in composite materials using generalised orthotropic pressure." *Continuum mechanics and thermodynamics* 32 (2020): 1217-1229. https://doi.org/10.1007/s00161-019-00835-6
[34] Mohd Nor, Mohd Khir, Rade Vignjevic, and James Campbell. "Modelling of shockwave propagation in orthotropic materials." *Applied Mechanics and Materials* 315 (2013): 557-561. https://doi.org/10.4028/www.scientific.net/AMM.315.557
[35] Ho, C. S., and M. K. Mohd Nor. "An experimental investigation on the deformation behaviour of recycled aluminium alloy AA6061 undergoing finite strain deformation." *Metals and Materials International* 27 (2021): 4967-4983. https://doi.org/10.1007/s12540-020-00858-8
[36] Ho, C. S., and M. K. Mohd Nor. "Tensile behaviour and damage characteristic of recycled aluminium alloys AA6061 undergoing finite strain deformation." *Proceedings of the Institution of Mechanical Engineers, Part C: Journal of Mechanical Engineering Science* 235, no. 12 (2021): 2276-2284. https://doi.org/10.1177/0954406220950349
[37] Ho, C. S., MK Mohd Nor, and M. S. A. Samad. "Modelling Temperature and Strain-Rate Dependence of Recycled Aluminium Alloy AA6061." *International Journal of Integrated Engineering* 14, no. 6 (2022): 135-145. https://doi.org/10.30880/ijie.2022.14.06.012
[38] Nor, MK Mohd. "Modeling of constitutive model to predict the deformation behaviour of commercial aluminum alloy AA7010 subjected to high velocity impacts." *ARPN J. Eng. Appl. Sci* 11, no. 4 (2016): 2349-2353.
[39] Taylor, Geoffrey Ingram. "The use of flat-ended projectiles for determining dynamic yield stress I. Theoretical considerations." *Proceedings of the Royal Society of London. Series A. Mathematical and Physical Sciences* 194, no. 1038 (1948): 289-299. https://doi.org/10.1098/rspa.1948.0081
[40] Whiffin, A. C. "The use of flat-ended projectiles for determining dynamic yield stress-II. Tests on various metallic materials." *Proceedings of the Royal Society of London. Series A. Mathematical and Physical Sciences* 194, no. 1038 (1948): 300-322. https://doi.org/10.1098/rspa.1948.0082
[41] Hawkyard, J. B. "A theory for the mushrooming of flat-ended projectiles impinging on a flat rigid anvil, using energy considerations." *International Journal of Mechanical Sciences* 11, no. 3 (1969): 313-333. https://doi.org/10.1016/0020-7403(69)90049-6
[42] Acosta, C. A., C. Hernandez, A. Maranon, and J. P. Casas-Rodriguez. "Validation of material constitutive parameters for the AISI 1010 steel from Taylor impact tests." *Materials & Design* 110 (2016): 324-331. https://doi.org/10.1016/j.matdes.2016.07.134
[43] Rakvåg, Knut Gaarder, Tore Børvik, Ida Westermann, and Odd Sture Hopperstad. "An experimental study on the deformation and fracture modes of steel projectiles during impact." *Materials & Design* 51 (2013): 242-256. https://doi.org/10.1016/j.matdes.2013.04.036

[44] Ho, Choon Sin, Muhamad Afandi Ab Rani, Mohd Khir Mohd Nor, Norzarina Ma'at, Mohamed Thariq Haji Hameed Sultan, Mohd Amri Lajis, and Nur Kamilah Yusuf. "Characterization of anisotropic damage behaviour of recycled aluminium alloys AA6061 undergoing high velocity impact." *International Journal of Integrated Engineering* 11, no. 1 (2019).

[45] Xiao, Xinke, Wei Zhang, Gang Wei, and Zhongcheng Mu. "Effect of projectile hardness on deformation and fracture behavior in the Taylor impact test." *Materials & Design* 31, no. 10 (2010): 4913-4920. https://doi.org/10.1016/j.matdes.2010.05.027

[46] Volkov, Grigori, Elijah Borodin, and Vladimir Bratov. "Numerical simulations of Taylor anvil-on-rod impact tests using classical and new approaches." *Procedia Structural Integrity* 6 (2017): 330-335. https://doi.org/10.1016/j.prostr.2017.11.050

[47] Johnson, Gordon R., and William H. Cook. "Fracture characteristics of three metals subjected to various strains, strain rates, temperatures and pressures." *Engineering fracture mechanics* 21, no. 1 (1985): 31-48. https://doi.org/10.1016/0013-7944(85)90052-9

[48] Macdougall, D. A. S., and J. Harding. "A constitutive relation and failure criterion for Ti6Al4V alloy at impact rates of strain." *Journal of the Mechanics and Physics of Solids* 47, no. 5 (1999): 1157-1185. https://doi.org/10.1016/S0022-5096(98)00086-6

[49] Meyer Jr, Hubert W., and David S. Kleponis. "Modeling the high strain rate behavior of titanium undergoing ballistic impact and penetration." *International Journal of Impact Engineering* 26, no. 1-10 (2001): 509-521. https://doi.org/10.1016/S0734-743X(01)00107-5

[50] Tham, C. Y., V. B. C. Tan, and Hwa-Pyung Lee. "Ballistic impact of a KEVLAR® helmet: Experiment and simulations." *International Journal of Impact Engineering* 35, no. 5 (2008): 304-318. https://doi.org/10.1016/j.ijimpeng.2007.03.008

[51] Peirs, Jan, Patricia Verleysen, Wim Van Paepegem, and Joris Degrieck. "Determining the stress–strain behaviour at large strains from high strain rate tensile and shear experiments." *International Journal of Impact Engineering* 38, no. 5 (2011): 406-415. https://doi.org/10.1016/j.ijimpeng.2011.01.004

[52] Dehkharghani, A. A. (2016). Tuning Johnson-Cook material model parameters for impact of high velocity, micron scale aluminum particles. Northeastern University.

[53] Kamarudin, Kamarul Azhar, Mohamed Nasrul Mohamed Hatta, Ranjhini Anpalagan, Noor Wahida Ab Baba, Mohd Khir Mohd Noor, Rosniza Hussin, and Ahmad Sufian Abdullah. "Seashell structure under binder influence." *Journal of Advanced Research in Fluid Mechanics and Thermal Sciences* 46, no. 1 (2018): 122-128.